

PLANT SCIENCES

Coactivation of antagonistic genes stabilizes polarity patterning during shoot organogenesis

Chunmei Guan^{1†}, Lingxia Qiao^{2†‡}, Yuanyuan Xiong^{1§}, Lei Zhang^{2*}, Yuling Jiao^{1,3,4*}

Spatiotemporal patterns of gene expression are instrumental to morphogenesis. A stable pattern interface, often between reciprocal-inhibiting morphogens, must be robustly maintained after initial patterning cues diminish, organ growth, or organ geometry changes. In plants, floral and leaf primordia obtain the adaxial-abaxial pattern at the shoot apical meristem periphery. However, it is unknown how the pattern is maintained after primordia have left the shoot apex. Here, through a combination of computational simulations, time-lapse imaging, and genetic analysis, we propose a model in which auxin simultaneously promotes both adaxial and abaxial domains of expression. Furthermore, we identified multilevel feedback regulation of auxin signaling to refine the spatiotemporal patterns. Our results demonstrate that coactivation by auxin determines and stabilizes antagonistic adaxial-abaxial patterning during aerial organ formation.

INTRODUCTION

The patterning of upstream regulatory genes directs tissue and organ morphogenesis. Extensive studies have identified various pattern formation mechanisms in distinct developmental processes in plants and animals. Stable maintenance of patterns is necessary for proper organ and tissue morphogenesis but is much less well understood. Neighboring morphogens are often antagonistic to each other, making pattern stabilization and maintenance a challenge. Furthermore, dynamic growth changes organ size and geometry, which may shield patterning cues and distort existing pattern fields. Control theory, devoted to the analysis of robust systems containing feedback controls, is a promising method for analyzing biological systems, including patterning and morphogenesis.

In plants, the development of aerial organ primordia such as leaf primordia and floral primordia requires precise patterning of the adaxial, middle, and abaxial domains, which has been widely used in studies focused on understanding patterning and morphogenesis (1–3). Leaf and floral organ primordia initiate at the periphery of the shoot apical meristem (SAM), which is prepatterned (4–6). Genes from the class III homeodomain-leucine zipper (HD-ZIPIII) family promote adaxial cell fate and are expressed in the center of the SAM, while *KANADI* (*KAN*) genes controlling abaxial cell fate are expressed outside the SAM in a ring-shaped domain surrounding it. When leaf and floral primordia initiate, they encompass and maintain both adaxial and abaxial domains (Fig. 1A). This prepattern is presumably specified by the SAM. For example, the transcription factor gene *WUSCHEL* (*WUS*) is expressed in the SAM center, but

its encoding protein was proposed to migrate into adjacent cells to inhibit *KAN1* and *KAN2* transcription (7).

Within each primordium, an interconnected gene regulatory network involving transcription factors and small RNAs functions together with the prepatterning HD-ZIPIII and *KAN1* proteins. This regulatory network determines the mutual repression of adaxial-promoting and abaxial-promoting genes (1–3). In particular, gradients of mobile small RNAs generate sharply defined target gene expression domains (8). The adaxial-abaxial prepattern establishes primordium polarity and functions together with the phytohormone auxin to define the middle domain between adaxial and abaxial cell layers (9). The middle domain is itself responsible for the formation and flattening of the leaf lamina (2, 10).

Although the adaxial-abaxial interface surrounding the SAM periphery forms a relatively steady realm, this interface moves with the primordium (Fig. 1A). Hence, the adaxial-abaxial interface within a primordium is relatively stable when the primordium grows and moves away from the SAM. How the patterning interface is maintained and stabilized in primordia remains unknown. Here, we combine mathematical modeling and experiments to show that auxin, in addition to promoting primordium initiation, maintains the adaxial-abaxial pattern. We used a seesaw model to demonstrate that simultaneous activation of mutually antagonistic genes maintains robust patterns. We also identified interconnected regulatory nodes within the network that act downstream of auxin.

RESULTS

Auxin maxima move the adaxial-abaxial interface

We first conducted time-lapse live imaging to quantify the location of the adaxial-abaxial interface in the shoot apex. The prepatterning expression domains of *REVOLUTA* (*REV*), an HD-ZIPIII gene, and *KAN1* have been shown to be similar in both vegetative and inflorescence SAMs (5, 6, 11). We imaged *Arabidopsis thaliana* inflorescence apices, as they are easily accessed and suffer minimal damage during confocal microscopy imaging at 24-hour intervals for up to 3 days.

Consistent with previous reports (11–13), the signal maxima of the auxin efflux carrier PIN-FORMED 1 (PIN1) were found to predict primordium initiation. PIN1 maxima formed within the *REV*

Copyright © 2022
The Authors, some
rights reserved;
exclusive licensee
American Association
for the Advancement
of Science. No claim to
original U.S. Government
Works. Distributed
under a Creative
Commons Attribution
NonCommercial
License 4.0 (CC BY-NC).

¹State Key Laboratory of Plant Genomics and National Center for Plant Gene Research (Beijing), Institute of Genetics and Developmental Biology, The Innovative Academy of Seed Design, Chinese Academy of Sciences, Beijing 100101, China.

²Beijing International Center for Mathematical Research, Center for Quantitative Biology, Peking University, Beijing 100871, China. ³State Key Laboratory of Protein and Plant Gene Research, Peking-Tsinghua Center for Life Sciences, School of Life Sciences, Center for Quantitative Biology, Peking University, Beijing 100871, China.

⁴College of Advanced Agricultural Sciences, University of Chinese Academy of Sciences, Beijing 100049, China.

*Corresponding author. Email: yuling.jiao@pku.edu.cn (Y.J.); zhangl@math.pku.edu.cn (L.Z.)

†These authors contributed equally to this work.

‡Present address: Department of Mechanical and Aerospace Engineering, Jacob's School of Engineering, University of California, San Diego, La Jolla, CA, USA.

§Present address: Geneplus-Beijing, Beijing 102206, China.

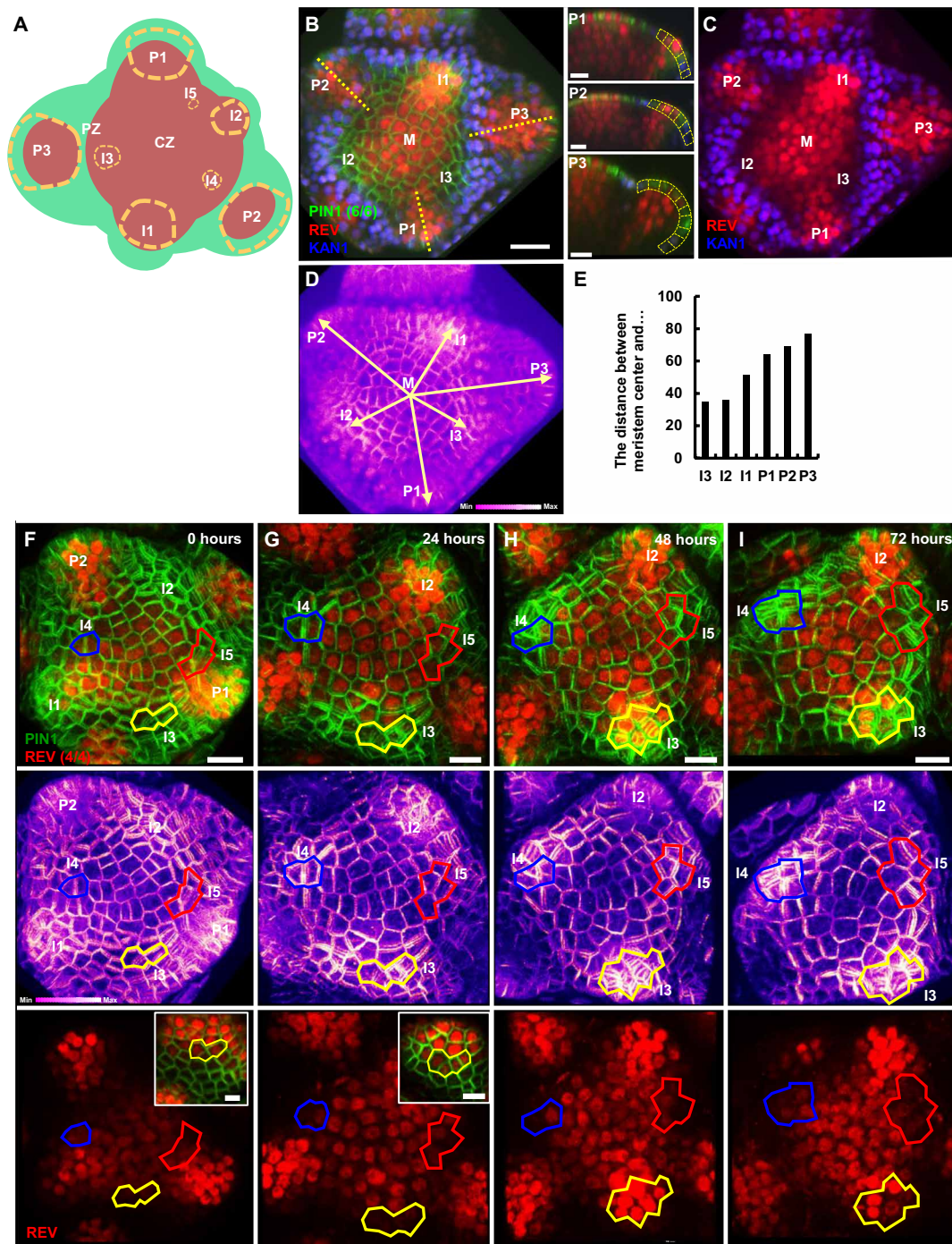


Fig. 1. PIN1 maxima converge with the REV-KAN1 expression interface and drive interface movement within primordia. (A) Model for lateral primordium initiation at the SAM. The lateral primordium initiates in the peripheral zone (PZ). I₅ to P₃ indicate primordia from youngest to oldest. (B) PIN1 signal (PIN1-CFP, green) combined with REV-2YPet (red) and KAN1-2GFP (blue) fluorescence signals in the epidermis of the inflorescence meristem. I₃ to P₂, primordia from youngest to oldest; (m/n) indicates that m in n biological repeats shows the displayed features. Optical longitudinal sections of primordia along the planes of sections, as depicted by dotted lines, are shown on the right. The primordia epidermal cells marked by PIN1 maxima are marked with yellow dotted lines. Scale bars, 20 μm. (C) REV-2xYPet and KAN1-2xGFP signal shown in (B). (D) Heatmap of PIN1-CFP fluorescence intensity. Yellow arrows indicate the distance between the center of the inflorescence meristem and floral primordia. (E) Distance between the center of the inflorescence meristem and floral primordia shown in (E). (F to I) One inflorescence apex imaged at four consecutive stages. The top panels show the PIN1 signal [PIN1-GFP (green fluorescent protein), green] combined with the REV-Venus signal (red) in the epidermis. Heatmaps of PIN1-GFP fluorescence intensity are shown in the middle panels. The REV-Venus (red) signal alone is shown in the lower panels. The insets show enlarged views of the I₃ primordium. Selected progenitor cells, their nearby progenitor cells, and their descendants are highlighted with colored lines. Note that each highlighted region starts with REV-positive cells but includes both REV- and KAN1-positive daughter cells after 72 hours. I₅ to P₂, primordia from youngest to oldest; (m/n) indicates that m in n biological repeats shows the displayed features. The positions of I₄ and I₅ at the first time points were inferred from later time points. Scale bars, 20 μm.

domain. Because of growth of the SAM, the same cells traveled toward the periphery (Fig. 1, B to I, and fig. S1). The *REV* and *KANI* domains were stably maintained before and after primordium emergence. However, once the *REV-KANI* expression interface met the PIN1 maxima, the interface moved together with the PIN1 maxima, resulting in protrusions of the *REV* domains at I_2 , which designates the second oldest incipient primordium (Fig. 1B and figs. S1 and S2). By P_2 , which denotes the second youngest primordium, the *REV* domain became isolated from the SAM by *KANI*-expressing cells (Fig. 1B). Thus, PIN1 maxima, which predict auxin convergence sites, do not rely on polarity patterning. However, it is reasonable to hypothesize that PIN1 maxima drive the movement of the interface of polarity domains outside of the SAM.

To test this idea, we imaged *REV* and *KANI* in *pin1-1* and *arf5-1* mutants, in which floral primordia are frequently absent but the SAM remains functional (13, 14). In both mutants, the *REV* expression domain was surrounded by the *KANI* domain at the SAM periphery. In contrast to wild-type SAMs, *REV* did not extend into the *KANI* domain in these mutant SAMs (fig. S3).

Seesaw model for the maintenance of polarity patterning in primordia

Alternative mechanisms likely exist to maintain the *REV-KANI* interface within a given primordium. To explore possible regulatory mechanisms, we proposed a seesaw model to measure the balance between *REV* and *KANI* based on known and speculated regulatory connections between polarity genes. The reciprocal inhibition between *KANI* and *REV* (15) causes the system to behave like a seesaw; when the expression level of *KANI* or *REV* is high, the expression of the other transcript in the pair is likely inhibited. Therefore, their relationship can be conceptualized as a seesaw; one end must go up whenever the other goes down. The seesaw concept has also been used to describe a two-module (i.e., a pluripotency module and a differentiation module) model for cell reprogramming (16). During early floral primordium development up to P_2 , three to six cell layers are present (Fig. 1B), whereas the leaf primordium consistently has six layers of cells (17). Therefore, we divided a primordium into 6 cell layers at time 0 (i.e., P_1) and set each of the first two cells to divide into identical daughter cells with unchanged gene expression levels at 24 and 48 hours, respectively, corresponding to the increase in cell layers from 6 to 10 along the adaxial-abaxial axis from P_1 to P_3 as shown in Fig. 1B. Then, we used ordinary differential equations to model gene expression dynamics in these cell layers. Each state variable denotes the concentration of the gene product of *KANI* or *REV* in each cell; communication among cells is achieved by diffusion of gene products. The interactions between genes were modeled by Hill functions. If gene i promotes gene j expression, the production rate caused by gene i is modeled by $v_j \frac{(X_i/K_{x \rightarrow y})^2}{1 + (X_i/K_{x \rightarrow y})^2}$ (see Materials and Methods for details), where X_i , v_j , and $K_{x \rightarrow y}$ are the gene i product, the maximal production rate of gene j product X_j , and the half-saturation value, respectively. Similarly, an inhibition is modeled by $v_j \frac{1}{1 + (X_i/K_{x \rightarrow y})^2}$. The degradation of the gene product is set to be a linear function of itself, i.e., $d_j X_j$, where d_j is the degradation rate.

However, integrating the reciprocal negative regulation between *KANI* and *REV* into a seesaw model was not sufficient to maintain the robust *REV-KANI* interface in the leaf primordium (simulation 1; Fig. 2A). The strong inhibitory influence of *KANI* on *REV*

maintains a low *REV* expression level, leading to a *KANI*-dominated domain. Our findings suggest that auxin convergence moves the patterning interface, so we next focused on auxin regulators of polarity genes and their interactions. For simulation 2, we included the following regulatory connections. MONOPTEROS (MP) promotes *PRESSED FLOWER* (*PRS*) and *WUSCHEL-RELATED HOMEBOX 1* (*WOX1*) expression (9), and *PRS* and *WOX1* induce *MP* expression (18). In the inflorescence meristem, *PRS* is expressed early during primordium formation (fig. S4). In addition, MP maintains the expression of its encoding gene by self-activation (19). Last, expression of *KANI* in the abaxial domain inhibits the expression of *PRS* and *WOX1* in the middle domain (10). Because there is no feedback regulation from *PRS* or *MP* to *REV* or *KANI*, the dynamics of *REV* and *KANI* were not affected by their inclusion in the model. As expected, the computational simulation indicated that the abaxial domain would encompass the entire primordium in this scenario (simulation 2; Fig. 2B), demonstrating that it does not accurately model primordium behavior.

We next considered potential positive regulation of *REV* expression by auxin (5). After adding MP activation of *REV* expression to the model, the new simulation maintained the adaxial domain, which eventually grew to encompass the abaxial domain and occupy the entire primordium (simulation 3; Fig. 2C). This growth can be predicted because *REV* activates *MP* expression so effectively that *KANI* is fully inhibited by *REV*. It has also been speculated that auxin inhibits *KANI* expression (5). After this assumption was added to the model, *KANI* expression was found to be even lower than that in simulation 4, resulting in a more rapid disappearance of the abaxial domain (simulation 4; Fig. 2D). In contrast, if we assume that auxin simultaneously promotes *KANI* and *REV* expression, the mutual inhibitory effects between *KANI* and *REV* are well balanced, leading to a stabilized pattern in which the *REV-KANI* interface is maintained within primordia (simulation 5; Fig. 2E). In addition to the *REV-KANI* pattern, we also explored how *MP* and *PRS* patterns evolve in simulations 2 to 5. In these models, we assume that the initial levels of *MP* and *PRS* are high in the middle cells (5, 9, 19). Our simulation of the dynamics of *MP* and *PRS* predicted that the expression levels of both *MP* and *PRS* would remain high in middle cells, while their expression levels in other cells would remain low (figs. S5 and S6). This predicted distribution of *MP* and *PRS* corresponds with experimental observations from studies of early primordia (5, 9, 19).

MP directly promotes *REV* and *KANI* expression

To assess the plausibility of the simulations, we tested the postulated regulation of *REV* and *KANI* expression by auxin. Among class A AUXIN-RESPONSE FACTORS (ARFs), MP plays a leading role in leaf development (9, 20). In the inflorescence SAM, the *MP* expression domain encompassed both the *REV* and *KANI* expression domains (Fig. 3, A and B). To investigate whether MP regulates *REV* and *KANI* expression, we used a transgenic line expressing *pMP:MPΔ-GR*, in which MPΔ, lacking domains III and IV and thus escaping auxin regulation, was fused to the rat glucocorticoid receptor (GR). Application of dexamethasone (Dex) induced the translocation of MPΔ-GR to the nucleus, allowing us to measure *REV* and *KANI* expression levels by reverse transcription quantitative polymerase chain reaction (RT-qPCR) (Fig. 3, C to E). We observed induction of *REV* and *KANI* expression in apices treated with Dex and cycloheximide (CHX), an inhibitor of protein biosynthesis, suggesting

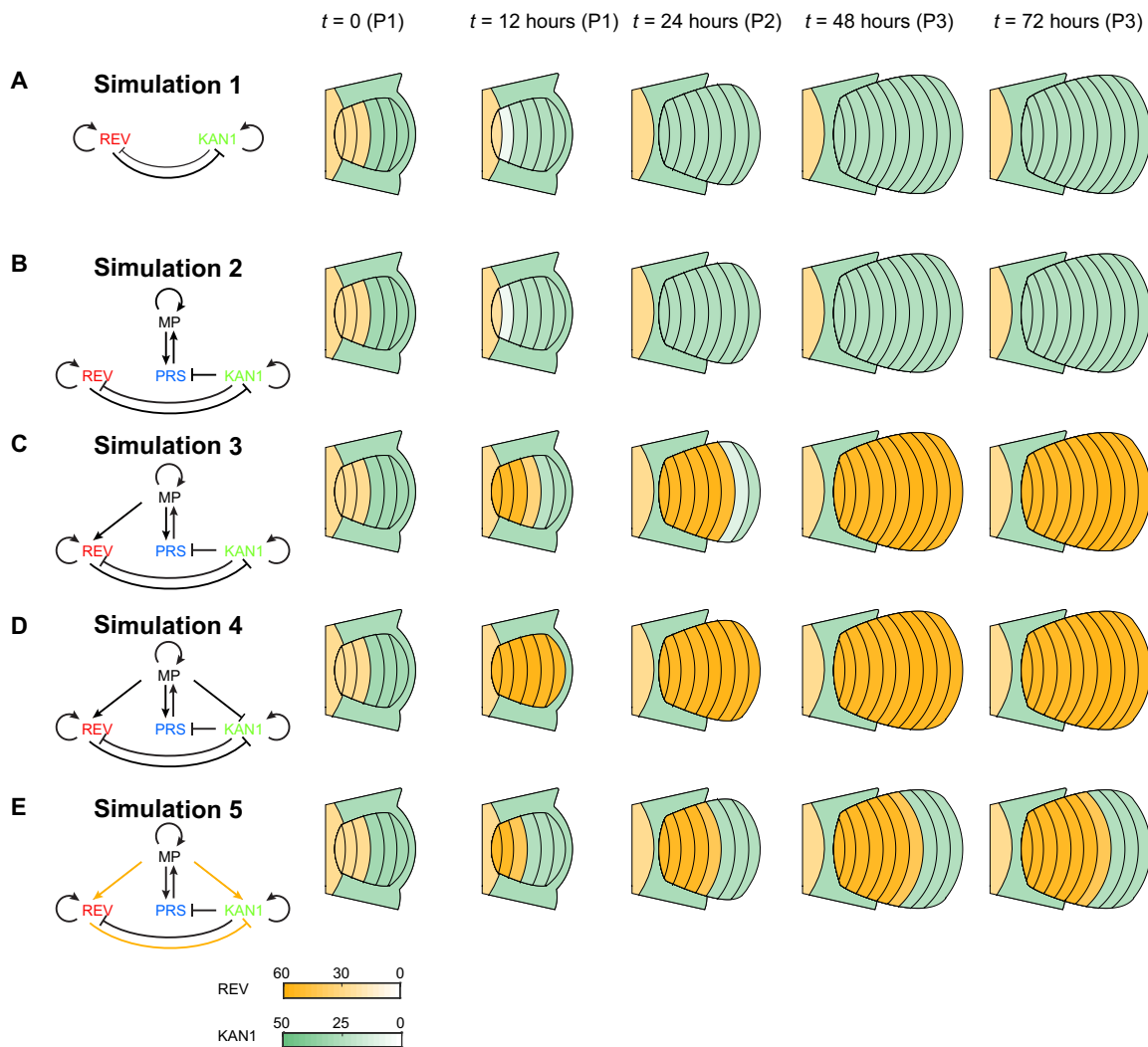


Fig. 2. Seesaw model simulations of polarity patterning based on known and speculated regulatory connections between polarity genes. (A to E) Gene regulatory networks (left) and corresponding dynamics of gene products (right). The entire region represents one primordium at the SAM periphery, divided into 6 to 10 cell layers as time evolves. The color of each cell layer is determined by the simulated expression levels of *REV* and *KAN1*. The regulatory relationships shown in orange in (E) were experimentally validated in this study. At $t = 72$ hours, the steady state is reached.

that *REV* and *KAN1* are likely direct targets of MP. The promoters of *REV* and *KAN1* contain multiple auxin-responsive elements (AuxREs), which constitute potential binding sites for MP (Fig. 3, F and G). In particular, we identified five AuxRE pairs, which are high-confidence MP binding sites (21), in the *REV* promoter region and two pairs in the *KAN1* promoter region. Chromatin immunoprecipitation (ChIP) assays at the *REV* promoter showed a strong association between MP-GFP [MP fused to green fluorescent protein (GFP)] and one region, as well as a weaker association with three other regions (Fig. 3H). We also detected an association between MP-GFP and two regions of the *KAN1* promoter, including one containing an AuxRE pair (Fig. 3I).

We next validated the transcriptional activation of the *REV* and *KAN1* promoters by MP through a transient transfection assay in protoplasts. MP Δ activated *pREV:LUC* and *pKAN1:LUC* reporters, as evidenced by strong luciferase activity (Fig. 3, J to L). Notably, the responsiveness of the *REV* promoter to MP Δ overexpression was

more than 10 times that of the *KAN1* promoter. Activation of the *REV* promoter by MP Δ decreased by half when the AuxREs shown by the ChIP experiments to be bound by MP were deleted (Fig. 3M). Similarly, when the AuxREs in the three bound regions in the *KAN1* promoter were each mutated or deleted, the resulting mutated promoters failed to respond to MP Δ (Fig. 3N). Further experiments indicated that all AuxREs are redundantly required for MP Δ activation, as demonstrated by the associated gradual reduction in luciferase activity as they were successively mutated or deleted (Fig. 3N). These results confirmed that the AuxRE region plays an important role in the regulation of *REV* and *KAN1* expression by MP. In agreement with these findings, the expression levels of *REV* and *KAN1* in inflorescences from the hypomorphic *mp-S319* mutant were markedly lower than those of wild-type inflorescences (Fig. 3O). Together, our experimental results indicate that MP positively regulates the expression of *REV* and *KAN1* by binding directly to their promoters.

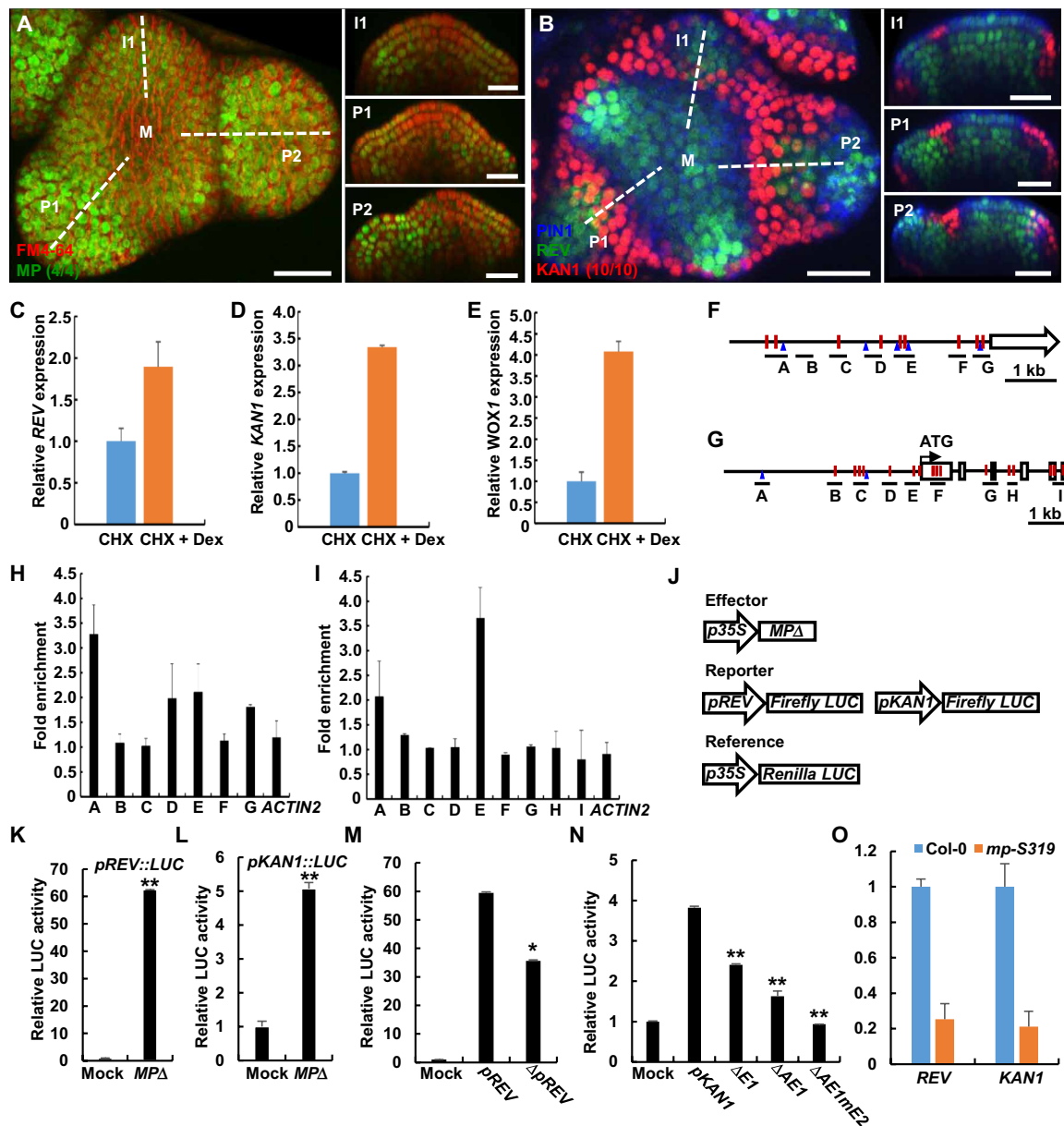


Fig. 3. MP directly up-regulates *KAN1* and *REV* expression. (A and B) Pattern of (A) MP-GFP (green) and (B) REV-2YPet (green) and KAN1-2GFP (red) abundance in the inflorescence meristem. Reconstructed views are shown on the left. Optical longitudinal sections through primordia I1 to P2 and the meristem center (along the white dashed line) are shown on the right. M, meristem; (m/n) indicates that *m* in *n* biological repeats shows the displayed features. Scale bars, 20 μ m. (C to E) RT-qPCR analysis of *REV* (C), *KAN1* (D), and *WOX1* (E) expression in *pMP:MPΔ-GR* inflorescence meristems after 4 hours of treatment with 50 μ M CHX in the absence or presence of 10 μ M Dex. Error bars indicate SD from three biological replicates. (F and G) Schematic diagram of the *REV* (F) and *KAN1* (G) genomic regions. Black boxes indicate exons. Vertical lines and triangles indicate AuxRE sites and pairs, respectively. The single AuxRE sites and pairs deleted or mutated in (M) and (N) are in blue. The underlying lines represent the regions amplified in chromatin immunoprecipitation (ChIP) assays. (H and I) ChIP enrichment of *REV* (H) and *KAN1* (I) genomic fragments using *pMP:MP-GFP* seedlings and an anti-GFP antibody. (J) Dual-luciferase reporter assay system applied in transiently transfected *Arabidopsis* protoplasts for the *pREV:LUC* (K) and *pKAN1:LUC* (L) reporters. A *35S:Renilla Luciferase* (*LUC*) reporter was used as an internal control. (K to N) Ratio of *Firefly LUC* to *Renilla LUC* activity in *Arabidopsis* protoplasts cotransfected with different reporter and effector combinations. (M) and (N) show the results of mutated *REV* (M) and *KAN1* (N) reporters and *MPΔ* effector combinations. Error bars indicate SD from three biological replicates. **P* < 0.05 and ***P* < 0.01. (O) RT-qPCR analysis of *REV* and *KAN1* expression in *mp-S319* inflorescence meristems. Error bars indicate SD from three biological replicates.

Auxin and MP modulate the spatial expression of *REV* and *KAN1*

We then tested the effects of MP and auxin on spatial gene expression by live imaging. For simulation 5, we perturbed its kinetic

parameters and found that the *REV-KAN1* pattern was maintained when any of the following conditions were met (fig. S7, left): The strength of the regulatory effect of MP on *REV* increased by no more than 40% of the original value (used in Fig. 2E and listed in

table S2, same below); the strength of the regulatory effect of MP on *KAN1* increased by no more than 50%; the strength of the regulatory effect of PRS on *MP* was between 60 and 120% of the original value; the basal *MP* production, which reflects auxin input, was between 20 and 100% of the original value. These results indicate that the balanced *REV-KAN1* partition is highly robust to perturbations, including variation in the strength of the auxin input (fig. S7). We experimentally tested this prediction by treating inflorescences with the synthetic auxin analog 2,4-dichlorophenoxyacetic acid (2,4-D), after which we imaged the *REV-KAN1* interface (Fig. 4, A and B). After 24 hours, we observed a slight enlargement of the *REV* domain at the expense of the *KAN1* domain at the shoot apex. Nevertheless, the *REV-KAN1* interface remained within the primordium. As shown by RT-qPCR analysis, the *KAN1* expression level increased 4 hours after Dex induction of *pMP:MPΔ-GR* inflorescences but returned to its original level 16 hours after induction (fig. S8).

We next crossed the *pMP:MPΔ-GR* transgenic line with a *pREV:REV-Venus* reporter line, which revealed that Dex treatment triggers

elevated *REV-Venus* accumulation (Fig. 4, C to F). To shield *KAN1* expression from the effects of HD-ZIPIII, we used a Cre/loxP-based system that allows conditional expression of *MPΔ-TagRFP* [*MPΔ* cloned in-frame and upstream of the red fluorescent protein gene (*RFP*)] after estradiol induction (22). After induction, cells accumulating *MPΔ-TagRFP* in the *KAN1* domain showed substantial up-regulation of *KAN1-GFP* expression (Fig. 4, G to H'). In addition, neighboring cells often displayed increased expression of *KAN1-GFP*, suggesting non-cell-autonomous effects, possibly due to activation of endogenous *MP* expression by ectopic *MPΔ-TagRFP*. We also generated specific deletions/mutations of the MP-bound AuxREs in the *KAN1* promoter, and we found that the *KAN1-GFP* expression level in the inflorescence meristems of the resulting *pKAN1m:KAN1-GFP* transgenic lines was decreased (Fig. 5, A to D). These results suggested that local *MP* overexpression is sufficient to enhance *REV* and *KAN1* expression.

As *MP* promotes *REV* expression, ectopic *REV* expression may partially rescue lost *MP* activity. To test this hypothesis, we crossed

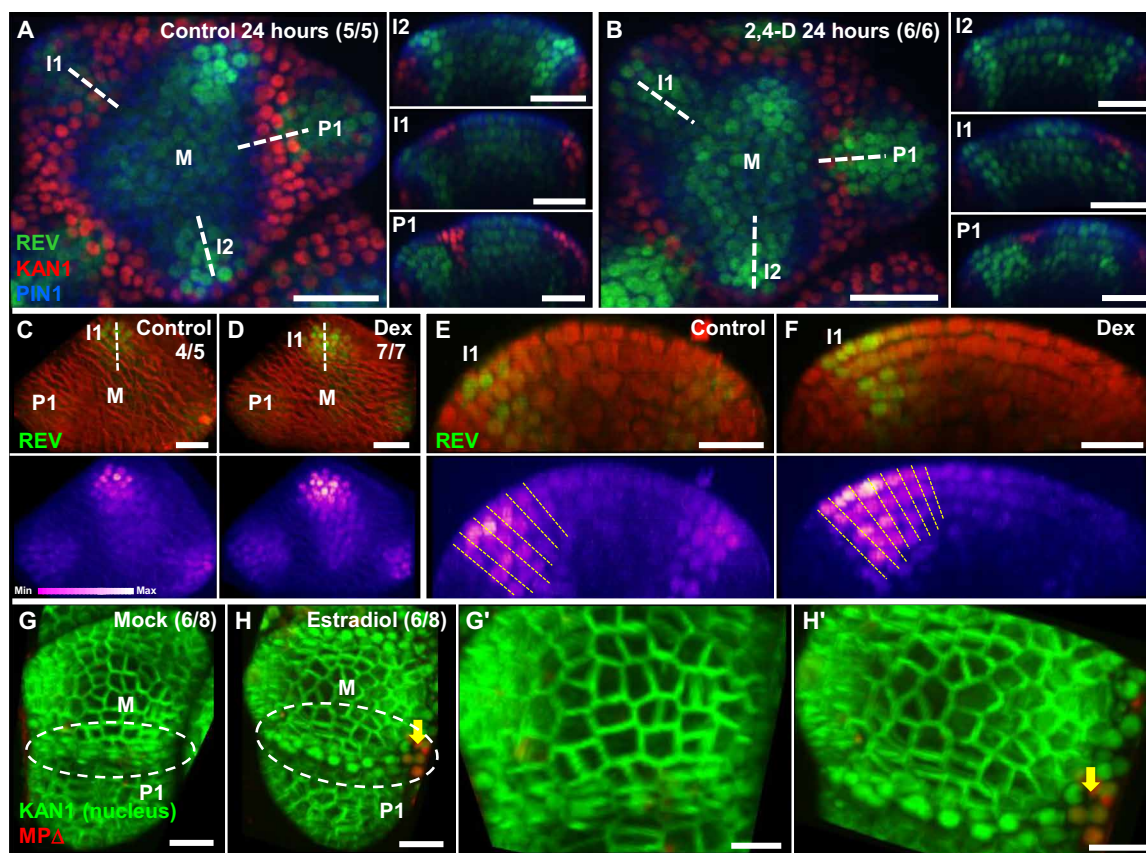


Fig. 4. MP and auxin regulate *REV* and *KAN1* expression in vivo. (A and B) Confocal imaging of the *REV-2YPet* (green) and *KAN1-2GFP* (red) signals under control (A) or 50 μ M 2,4-D treatment (B) for 24 hours. Optical longitudinal sections of *I*₂ to *P*₁ along the white dotted lines are shown at the right. M, meristem; (m/n) indicates that m in n biological repeats shows the displayed features. Scale bars, 20 μ m. (C and D) Confocal imaging of the *REV-Venus* (green) signal in a *pMP:MPΔ-GR* inflorescence meristem under control (C) or 10 μ M Dex treatment (D) for 12 hours. The cell outlines were imaged by FM4-64 stain (red). The fluorescence intensity heatmap of the *REV-Venus* signal is shown at the bottom. Fluorescence intensity is shown from purple (low) to white (high), and (m/n) indicates that m in n biological repeats shows the displayed features. Scale bars, 20 μ m. (E and F) Optical longitudinal sections of an *I*₁ primordium along the white dotted lines shown in (C) (E) and (D) (F), respectively. The fluorescence intensity heatmap of the *REV-Venus* signal is shown at the bottom. Fluorescence intensity is shown from purple (low) to white (high). The layers of Venus-expressing cells are marked with yellow dotted lines. Scale bars, 20 μ m. (G and H) Confocal imaging of an inflorescence meristem expressing *KAN1-GFP* (green signal in the nucleus) before (G) and 6 days after induction of *MPΔ-TagRFP* (red) clones (H). The yellow arrow indicates induced *MPΔ-TagRFP* clones, and (m/n) indicates that m in n biological repeats shows the displayed features. Scale bars, 20 μ m. (G' and H') Enlarged view of the region marked by the oval dashed line in (G) and (H), respectively. Scale bars, 20 μ m.

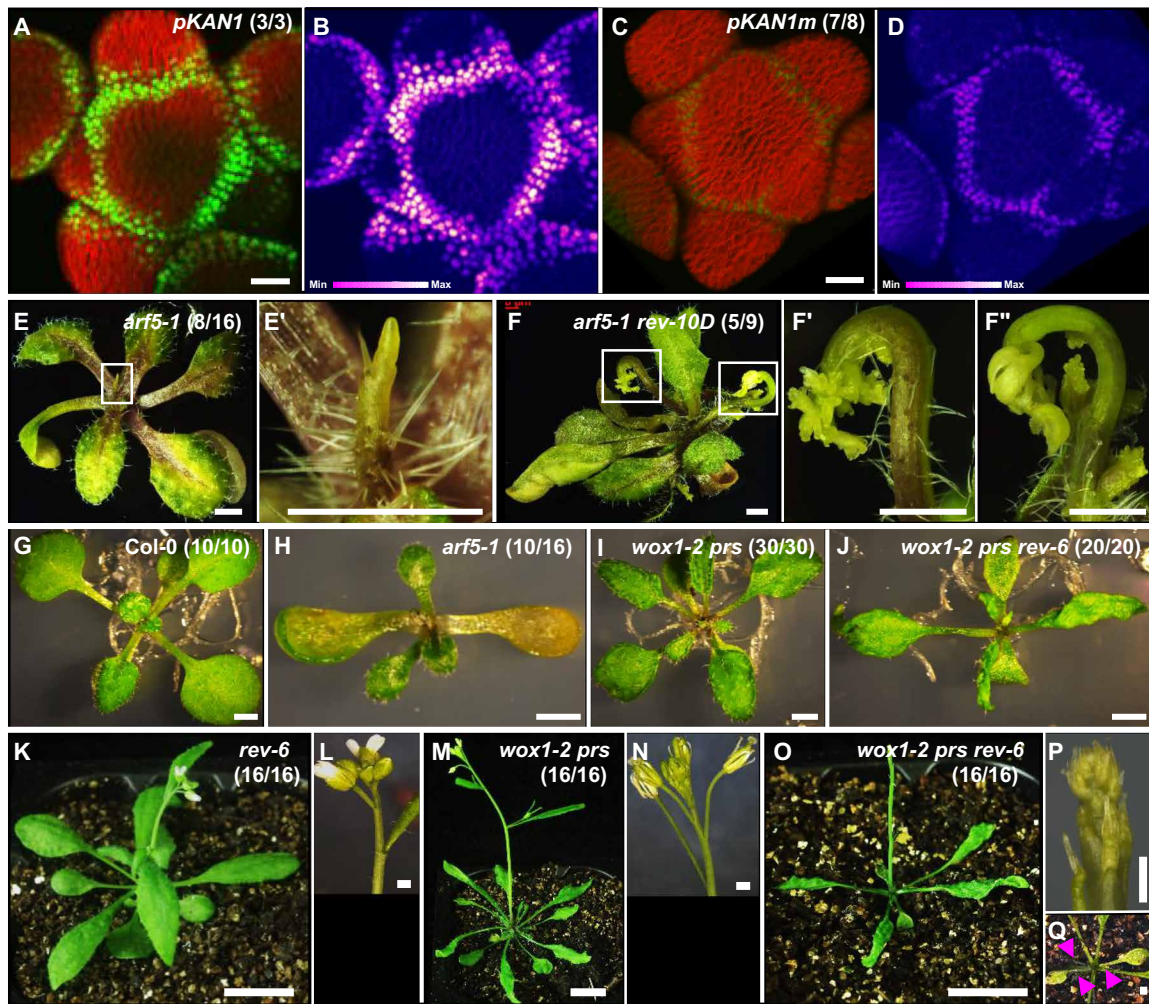


Fig. 5. MP and auxin regulate REV and KAN1 expression in vivo. (A to D) Confocal imaging of inflorescence meristems expressing *pKAN1:KAN1-GFP* (A and B) or *pKAN1m:KAN1-GFP* (C and D). Heatmaps of GFP fluorescence intensity are shown in (B) and (D), respectively. Scale bars, 20 μ m. (E) Forty-day-old *arf5-1* plant grown on Murashige and Skoog (MS) medium. Scale bar, 1 mm. (E') Enlarged view of the *arf5-1* inflorescence indicated in the white square in (E) showing a naked shoot apex. Scanning electron microscopy (SEM) images are shown in fig. S8. Scale bar, 1 mm. (F) Forty-day-old *arf5-1 rev-10D* plant grown on MS medium. Scale bar, 1 mm. (F' and F'') Enlarged view of the *arf5-1 rev-10D* inflorescence indicated in the white square in (F) showing primordia formation. SEM images are shown in fig. S8. Scale bars, 1 mm. (G) Twelve-day-old Col-0 seedling. Scale bar, 1 mm. (H) Twelve-day-old *arf5-1* seedling. Scale bar, 1 mm. (I) Twelve-day-old *wox1-2 prs* double-mutant seedling. Scale bar, 1 mm. (J) Twelve-day-old *wox1-2 prs rev-6* triple-mutant seedling. Scale bar, 1 mm. (K) Thirty-day-old *rev-6* plant. Scale bar, 10 mm. (L) Inflorescence of the *rev-6* plant in (K). Scale bar, 1 mm. (M) Thirty-day-old *wox1-2 prs* double-mutant plant. Scale bar, 10 mm. (N) Inflorescence of the *wox1-2 prs* plant in (M). Scale bar, 1 mm. (O) Thirty-day-old *wox1-2 prs rev-6* triple-mutant plant. Scale bar, 10 mm. (P) Inflorescence of the *wox1-2 prs rev-6* plant in (O). Scale bar, 0.5 mm. (Q) Rosette leaves of the *wox1-2 prs rev-6* plant in (O). Purple arrowheads indicate needle-like leaves. Scale bar, 1 mm. In each panel, (m/n) indicates that *m* in *n* biological repeats shows the displayed features, and in (E) and (F), the rest did not bolt.

the *arf5-1* single mutant, harboring a transferred DNA insertion in MP (also named ARF5), with *rev-10D*, a gain-of-function *REV* mutant. We observed organ-like protrusions in the inflorescences of *arf5-1 rev-10D* double mutants (Fig. 5, E to F'', and fig. S9), indicating that *rev-10D* partially rescues the pin-like inflorescence phenotype of *arf5-1*. Similar to *REV*, *PRS* and *WOX1* are also up-regulated by MP, prompting us to generate the *wox1-2 prs rev-6* triple mutant. Floral primordia were frequently replaced by filamentous structures in *wox1-2 prs rev-6* inflorescences (Fig. 5, O to Q). We also analyzed vegetative growth and observed reduced leaf number and narrow leaves in *wox1-2 prs rev-6* plants (Fig. 5, H to J), which were not

shown by either *wox1-2 prs* or *rev-6* plants. In addition, we observed a high frequency of needle-like rosette leaves in *wox1-2 prs rev-6* plants (Fig. 5Q), which is also found in *arf5-1* plants (9). These results suggest that *REV* and *PRS/WOX1* act synergistically in leaf and floral primordia development, which correlates with the maintenance of the *REV-KAN1* interface (see below).

Additional regulatory relationships within the gene regulatory network underlying primordia morphogenesis

We performed experiments to identify additional regulatory relationships within the gene regulatory network underlying

inflorescence development. To this end, we measured the gene expression of a Dex-inducible *p35S:FLAG-GR-REVd* transgenic line expressing a microRNA-resistant version of the *REV* mRNA transcript after short-term Dex treatment (Fig. 6, A to D). Dex treatment for 4 hours reduced the transcript level of *KAN1*, suggesting that *REV* directly represses *KAN1* expression (Fig. 6A). In contrast, Dex treatment for 4 hours increased the transcript levels of *WOX1*, *PRS*, and *MP* (Fig. 6, B to D). We also used *pWOX1:WOX1-GR* transgenic lines to show that *WOX1* represses *KAN1* expression after Dex treatment (Fig. 6F) but has no obvious effect on *REV* expression (Fig. 6E). Independently, we established that *WOX1* and *PRS* promote *pREV:LUC* expression (Fig. 6, G and H) and

inhibit *pKAN1:LUC* expression (Fig. 6, G and I) using the transient protoplast transfection assay.

We then confirmed these regulatory relationships in planta. In comparison with the fluorescence intensity of *pPRS:GFP* in wild-type inflorescence meristems, the fluorescence intensity was lower in the inflorescence meristems of *rev-5*, while it was higher in those of *rev-10D* (Fig. 6J and fig. S11). Our findings and previous work (10) indicate that reciprocal inhibitory relationships between *PRS*/*WOX1* and *KAN1* influence their expression levels. To confirm these regulatory relationships in vivo, we imaged the *KAN1*-GFP fluorescence pattern in inflorescence meristems of the *wox1-2 prs* double mutant (Fig. 6K and fig. S11). In *wox1-2 prs* inflorescences,

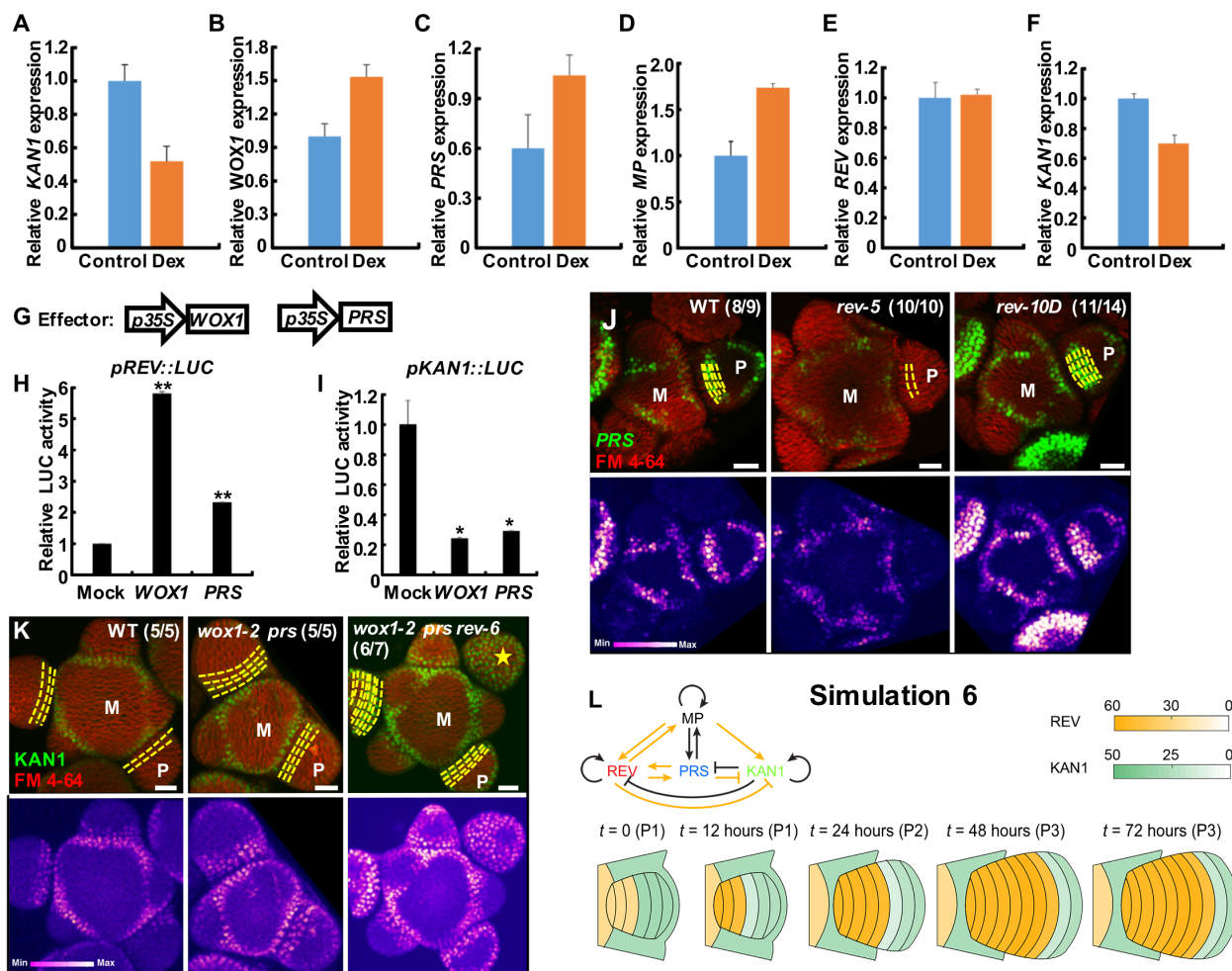


Fig. 6. MP, REV, WOX1/PRS, and KAN1 form a gene regulatory network containing feedback loops. (A to D) qRT-PCR analysis of *KAN1* (A), *WOX1* (B), *PRS* (C), and *MP* (D) expression in *p35S:FLAG-GR-REVd* inflorescence meristems after 4 hours of 10 μ M Dex treatment. Error bars indicate the SD from three biological replicates. (E and F) qRT-PCR analysis of *REV* and *KAN1* expression in *pWOX1:WOX1-GR* inflorescence meristems treated as above. Error bars indicate the SD from three biological replicates. (G) Dual-luciferase reporter assay system applied in transiently transfected *Arabidopsis* protoplasts for the *pREV:LUC* (H) and *pKAN1:LUC* (I) reporters. (H and I) Ratio of *Firefly* LUC to *Renilla* LUC activity in *Arabidopsis* protoplasts. Error bars indicate the SD of three biological replicates. * $P < 0.05$ and ** $P < 0.01$. (J and K) Inflorescence meristems showing signals of (I) *pPRS:SV40-GFP* expression (green) in wild-type (WT), *rev-5*, and *rev-10D* plants and (J) *KAN1*-GFP expression (green) in WT, *wox1-2 prs*, and *wox1-2 prs rev-6* plants. The reconstructed view of the inflorescence meristems shows *pPRS:SV40-GFP* or *KAN1*-GFP and FM4-64 staining (red) on the top. The fluorescence intensity heatmaps of the *pPRS:SV40-GFP* or *KAN1*-GFP signal are shown at the bottom. The layers of GFP-expressing cells are marked with yellow dotted curve lines. Fluorescence intensities are coded purple to white, corresponding to increasing intensity levels. Quantifications of fluorescence intensities of primordia marked with "P" are in fig. S11. The yellow star in (K) indicates a floral meristem almost completely covered by the *KAN1*-GFP signal in the triple mutant. (m/n) indicates that *m* in *n* biological repeats shows the displayed features. Scale bars, 20 μ m. (L) The computational simulation including the regulatory relationships in (Fig. 3D) and the regulatory relationships between *WOX* genes and *REV/KAN1*. The yellow lines indicate regulatory relationships identified in this study.

KAN1-GFP fluorescence was detected over a larger domain and with higher intensity in comparison with that of wild-type inflorescences. The KAN1-GFP fluorescence intensity was further increased, both spatially and quantitatively, in the *wox1-2 prs rev-6* triple mutant. Although other redundant HD-ZIP IIIs exist, KAN1-GFP fluorescence occupied most of the observed floral primordia (Fig. 6K). Considered together, these results show that PRS/WOX1 and REV share synergistic functions and inhibit KAN1 expression. Multiple feedback loops therefore exist in the gene regulatory network underlying primordia morphogenesis (Fig. 6L).

We updated the seesaw model by adding the newly identified regulatory mechanisms described above (simulation 6; Fig. 6L). The REV-KAN1 interface remained in the primordium, as seen previously in simulation 5. However, in contrast with simulation 5, the REV domain of simulation 6 was one cell layer larger at the expense of the KAN1 domain. A careful comparison with our imaging results (Fig. 1B) indicated that, in comparison with simulation 5, simulation 6 better recapitulates in planta expression patterns (fig. S7). The additional regulatory relationships in the model refine, but do not eliminate, the REV-KAN1 interface, suggesting that the regulatory relationships included in simulation 5 play central roles in maintaining it.

Furthermore, we tested the robustness of the model. First, we performed a sensitivity analysis for the model used in simulation 6 by varying one kinetic parameter while fixing others. For each kinetic parameter, we calculated the pattern at $t = 1200$ hours (the time at which a steady state is reached), and the fold change that stabilized the REV-KAN1 pattern was recorded (fig. S10, A and B). This model was found to be robust to maintain the REV-KAN1 pattern where the KAN1 domain occupies the last two cell layers (green bars in fig. S10B) or three cell layers (blue bars in fig. S10B). Besides, we plotted the REV-KAN1 patterns when changing the strength of REV to MP or KAN1 to MP (fig. S10C): When $K_{MP \rightarrow REV}$, the half-saturation value for the link from MP to KAN1, increased by 100%, the REV-KAN1 pattern was maintained, but the REV-KAN1 pattern disappeared when $K_{MP \rightarrow REV}$ decreased by 20% (fig. S10C). This result suggests that the REV-KAN1 pattern is robust to weak REV activation by MP but not robust to a strong REV activation by MP. In contrast, the REV-KAN1 pattern is robust to strong KAN1 activation by MP rather than weak activation. The above analysis focused on the robustness of simulation 6, and then we compared the robustness of simulation 6 to that of simulation 5 with regard to MP activity (fig. S7). We found that the pattern maintenance capability of simulation 6 was less robust than that of simulation 5, especially when the activation from MP to REV has been increased or activation from MP to KAN1 has been decreased (the first two columns in fig. S7). However, under weak activation from MP to REV or strong activation from MP to KAN1, simulations 5 and 6 are both robust. Both simulations are more robust to the regulatory strength from PRS to MP and to reduced MP activity (the last two columns in fig. S7). These results suggest that the additional regulatory relationships had limited effects on the robustness of the model.

Last, the accuracy of the predictions of the seesaw model was assessed. We changed the model according to the results shown in Fig. 6 (J and K), i.e., we modeled *rev-5*, *rev-10D*, *wox1-2 prs*, and *wox1-2 prs rev-6*. The *rev-5* mutant was modeled by constantly setting the REV amount to zero; *rev-10D* was modeled by setting the basal production rate of REV to 70 (or higher, whereas the value used in Fig. 2 is 60); *wox1-2 prs* was modeled by setting PRS amount

to zero; and *wox1-2 prs rev-6* was modeled by setting both PRS and REV to zero. The simulation results are shown in fig. S12. Deletion of REV slightly decreased the expression level of PRS, whereas a high REV expression level resulted in a high PRS expression level and an expansion of the expression domain. The predictions of the model regarding PRS expression levels are consistent with the results in Fig. 5I. In addition, the REV-KAN1 pattern was stable when PRS was deleted, while deleting PRS and REV simultaneously destroyed the REV-KAN1 pattern, leading to a KAN1-dominated pattern. These predictions regarding the REV-KAN1 pattern are also consistent with the experimental data in Fig. 6K.

DISCUSSION

Patterning of spatial gene expression often determines the creation of anatomical forms, i.e., morphogenesis. The emergence and maintenance of gene expression patterns are essential biological processes. However, morphogens often have reciprocal inhibitory relationships, and the mechanisms underlying the maintenance of robust gene expression patterns are not well understood.

Through multiple simulations using a seesaw model, we explored the effects of changes in regulatory mechanisms on the balance between antagonistic adaxial-promoting and abaxial-promoting genes. We also found through experimentation that auxin signaling serves as an upstream signal to maintain and stabilize the adaxial-abaxial interface, which is achieved by the simultaneous activation of both adaxial and abaxial genes. The simultaneous activation of antagonistic downstream genes is essential to robust pattern maintenance. We found that the adaxial-abaxial pattern was maintained after exogenous auxin treatment. Incorporating additional regulatory relationships into the model only refined the domain size (simulation 6), whereas removing regulatory relationships within the core network erased the existing pattern (simulations 1 to 4). We speculate that simultaneous activation of antagonistic genes may constitute a conserved mechanism to initiate and maintain gene expression patterns in a wide range of developmental processes.

MATERIALS AND METHODS

Growth conditions

Plants were grown in soil under constant light at 22°C. For live imaging of inflorescence primordia and quantitative analysis of gene expression, plants were grown at 22°C under constant light conditions until they had produced five siliques. For ChIP assays, seedlings were grown under long-day conditions (16 hours of light/8 hours of dark) on growth medium [half-strength Murashige and Skoog (MS), 1% (w/v) sucrose, and 0.8% (w/v) agar (pH 5.8)] at 22°C for 2 weeks.

Plant materials

The *Arabidopsis* (*A. thaliana*) accessions Columbia (Col-0) and Landsberg *erecta* (*Ler*) were used as the wild types. The *arf5-1*, *mp-S319* (23), *wox1-2 prs* (24), *rev-5* (25), and *rev-10D* (26) mutants used in this study are in the Col-0 background. The *rev-6* (25) mutant is in the *Ler* background. The transgenic lines *pPRS:SV40-3GFP* (27), *pMP:MP-GFP* (28), *pMP:MPΔ-GR* (9), and *p35S:FLAG-GR-REVd* (29) are in Col-0, and *pKAN1:KAN1-GFP* (11), *pREV:REV-Venus* *pPIN1:PIN1-GFP* (11), and *pREV:REV-2YPet pKAN1:KAN1-2GFP pPIN1:PIN1-CFP* (5) are in *Ler*.

Construction of transgenic plants

To construct the *pKANI:KAN1-GFP* vector, an 8758–base pair (bp) *KAN1* genomic fragment (a 5033-bp promoter and the 3725-bp genomic region until the stop codon, which was not included) was amplified by PCR using primers KAN1-F and KAN1-R (listed in table S1) and inserted into BJ36 between the Eco RI and Sma I restriction sites upstream of the coding sequence for *GFP*. The *pKANI:KAN1-GFP* cassette was then cloned into pMOA34 using the Not I site. To obtain *pKAN1m:KAN1-GFP*, the mutated *KAN1* promoter was amplified from the $\Delta AE1mE2pKAN1:LUC$ construct (described in “Transient transfection in protoplasts” below) and cloned into BJ36 upstream of *GFP* with the *KAN1* genomic sequence through Gibson assembly. The *pKAN1m:KAN1-GFP* cassette was then cloned into pMOA34 using the Not I site. These two constructs were transformed into Col-0 plants, and more than 10 stable transgenic lines were characterized for each construct.

To generate *pATML1:XVE-CRE*, a 3382-bp *ATML1* promoter fragment was amplified by PCR and assembled into the pCAM-BIA1300 vector through Gateway recombination. For the pMOA34-*pUBQ10-loxP-GUS-35S-polyA-loxP-MPA-TagRFP* construct, a 2389-bp *UBQ10* promoter fragment up to the start codon and a 3461-bp genomic fragment for the *MP* coding region were used. The construction process was described in the work of Bhatia *et al.* (19). These two constructs were then transformed into the marker line *pREV:REV-2YPet pKAN1:KAN1-2GFP pPIN1:PIN1-CFP*. Crosses were then performed between transgenic lines harboring each construct, whose F₁ progeny were used for live imaging.

RNA extraction and RT-qPCR

Total RNA was extracted from inflorescences using the AxyPrep Multisource Total RNA Miniprep Kit (Axygen) according to the manufacturer’s instructions. For experiments including Dex and CHX treatment, transgenic inflorescence apices were treated with 10 μ M Dex alone or with 10 μ M CHX for 4 hours. First-strand complementary DNA (cDNA) was synthesized using TransScript One-Step gDNA Removal and cDNA synthesis SuperMix (TransGen) and then used as the template for qPCR. qPCR was performed on a Bio-Rad CFX96 real-time PCR detection system using the KAPA SYBR FAST qPCR kit (KAPA Biosystems). The relative expression of target genes was normalized to the *ACTIN2* (At3g18780) level. All primers used in RT-qPCR are listed in table S1.

ChIP-PCR analysis

Two-week-old *pMP:MP-GFP* transgenic seedlings were harvested and frozen in liquid nitrogen. Five-gram samples of the seedlings were used in ChIP experiments. ChIP was performed as previously described (30). Immunoprecipitations were performed using anti-GFP antibodies. Enrichment was calculated relative to a no-antibody control experiment. qPCR was conducted using the precipitated DNA as the template to determine enrichment. Three independent biological replicates were analyzed for each ChIP analysis. All primers used in ChIP-PCR are listed in table S1.

Transient transfection in protoplasts

The transient transfection of *Arabidopsis* leaf protoplasts was performed as previously described (31). The *p35S:MPA* construct was described in the work of Guan *et al.* (9). For the *p35S:WOX1* and *p35S:PRS* constructs, full-length coding sequences of *WOX1* and *PRS* were amplified from *Arabidopsis* cDNA using the primers

WOX1-F/WOX1-R and *PRS-F/PRS-R*, respectively, before cloning into the pUC19-p35S-FLAG vector at the Kpn I (5’ end) and Bst BI (3’ end) sites. To construct *pREV:LUC*, a 4855-bp *REV* promoter fragment up to the translation start codon was amplified by PCR and inserted into pUC19 at the Eco RI and Sac I sites upstream of firefly *LUC*. To generate the $\Delta pREV:LUC$ construct, a 104-bp sequence in region A (tgtcgcttgt.....caagtgtctc), a 219-bp sequence in region D (gcaactgtgt.....gaagaggttt), 137- and 27-bp sequences in region E (tttggttcgt.....tcagagacag, acgacattga.....tgcatgtcga), and a 51-bp sequence in region G (tgtcgttggg.....ctttgtctg) were deleted from *pREV:LUC*. To generate *pKAN1:LUC*, a 5033-bp *KAN1* promoter fragment up to the translation start codon and a 132-bp fragment of the downstream coding region were amplified by PCR and inserted into pUC19 at the Eco RI and Sac I sites upstream of *LUC*. To generate the $\Delta E1pKAN1:LUC$ construct, a 21-bp sequence (aaatctttcagacaccctttt) in region E was deleted from *pKAN1:LUC*. To generate the $\Delta AE1pKAN1:LUC$ construct, a 47-bp sequence in region A (aactcttat.....ttgttttctt) was deleted from *\Delta E1pKAN1:LUC*. To generate the $\Delta AE1mE2pKAN1:LUC$ construct, the sequence “TCT,” corresponding to the second *KAN1* codon, was mutated to “AGC” without changing the encoded amino acid in $\Delta AE1pKAN1:LUC$.

Chemical treatments

For auxin treatment before live imaging, a 5 μ M 2,4-D solution containing 0.01% (v/v) Silwet-77 as a surfactant was applied to the primary inflorescence apex twice over 24 hours. For Dex treatment before live imaging, a 10 μ M Dex solution containing 0.01% (v/v) Silwet-77 was applied to the primary inflorescence apex once for 12 hours. For estradiol treatment, *pATML1>>MPA-TagRFP* inflorescence apices were immersed in a 20 μ M estradiol solution containing 0.01% Silwet-77 once and then grown for 6 days.

Live imaging

All live imaging experiments were performed using a Nikon A1+ confocal laser scanning microscope equipped with 40 \times and 60 \times water dipping lenses. To dissect inflorescence meristems, siliques and mature flowers were dissected away with fine forceps. Each dissected inflorescence apex with a short stem remaining was then placed into dissecting medium [3% (w/v) agarose], and the remaining floral primordia (older than needed) were carefully removed using a fine needle tip under a stereomicroscope (Nikon, SMZ18). After dissection, FM4-64 (10 μ g/ml; Thermo Fisher Scientific) was applied to the apex for 10 min. The inflorescence apex was then mounted in imaging medium [half-strength MS medium topped with 1% (w/v) agarose] and submerged in water for imaging. For time-lapse live imaging, the water was discarded, and samples were transferred back to new growth medium under normal growth conditions after each imaging session.

Confocal microscopy and optical microscopy

Confocal images were taken with a Nikon A1+ confocal laser scanning microscope. Excitation and detection wavelengths for CFP, Venus, GFP, YPet, TagRFP, and FM4-64 were as previously described (32). All images were scanned with 1024 \times 1024 pixel resolution. All optical photographs were taken with a Nikon SMZ1000 stereoscopic microscope equipped with a Nikon DS-Ri1 camera head.

Mathematical modeling

In our model, the number of cell layers increase with time: At time 0, six cells are aligned horizontally in a one-dimensional space that

represents the adaxial-abaxial axis; at time 24 hours, the first cell on the left-hand side divides into identical daughter cells whose gene expression levels are the same as the mother cell, and so does the cell near the first cell; at 48 hours, the first two cells divide again following the rule at 24 hours. This process corresponds to the 6- to 10-cell layer along the adaxial-abaxial axis from P_1 to P_3 . We assumed that gene products are distributed uniformly within each cell, and we used the subscript i to denote the gene product concentration in the i th cell. For example, $[REV_2]$ represents the concentration of the *REV* gene product (REV protein) in the second cell. To incorporate the cell-cell interactions caused by diffusion, each gene product is assumed to diffuse between neighboring cells following Fick's first law. Besides, in each cell, the interactions between genes are modeled by the Hill function: If gene x promotes the expression of gene y , then the production rate of gene x product is modeled by $v_x \frac{([x]/K_{x \rightarrow y})^2}{1 + ([x]/K_{x \rightarrow y})^2}$ where v_x is the maximal production rate for gene x product and $K_{x \rightarrow y}$ is the half-saturation value; likewise, if gene x inhibits the expression of gene y , then the production rate of gene x product is modeled by $v_y \frac{1}{1 + ([x]/K_{x \rightarrow y})^2}$. Furthermore, if multiple genes regulate the same target gene, then we assume that activating links are operated in OR logic and inhibiting links AND logic. On the basis of the above assumptions, the dynamics of gene products in simulation 6 can be described with the following equations

$$\left\{ \begin{aligned} \frac{d[REV_i]}{dt} &= k_{b,REV} + v_{rev} \left(\frac{([REV_i])^2}{K_{REV \rightarrow REV}} + \frac{([MP_i])^2}{K_{MP \rightarrow REV}} + \frac{([PRS_i])^2}{K_{PRS \rightarrow REV}} \right) \frac{1}{1 + \left(\frac{[REV_i]}{K_{REV \rightarrow REV}} \right)^2 + \left(\frac{[MP_i]}{K_{MP \rightarrow REV}} \right)^2 + \left(\frac{[PRS_i]}{K_{PRS \rightarrow REV}} \right)^2} - d_{REV} [REV_i] + D([REV_{i+1}] + [REV_{i-1}] - 2[REV_i]) \\ \frac{d[MP_i]}{dt} &= k_{b,MP} + v_{MP} \left(\frac{([MP_i])^2}{K_{MP \rightarrow MP}} + \frac{([PRS_i])^2}{K_{PRS \rightarrow MP}} + \frac{([REV_i])^2}{K_{REV \rightarrow MP}} \right) - d_{MP} [MP_i] \\ &\quad + D([MP_{i+1}] + [MP_{i-1}] - 2[MP_i]) + k_{MP} \chi_{\{3,4\},\{5,6\},\{7,8\}}(i) \\ \frac{d[PRS_i]}{dt} &= k_{b,PRS} + v_{PRS} \left(\frac{([MP_i])^2}{K_{MP \rightarrow PRS}} + \frac{([REV_i])^2}{K_{REV \rightarrow PRS}} \right) \frac{1}{1 + \left(\frac{[MP_i]}{K_{MP \rightarrow PRS}} \right)^2 + \left(\frac{[REV_i]}{K_{REV \rightarrow PRS}} \right)^2} - d_{PRS} [PRS_i] \\ &\quad + D([PRS_{i+1}] + [PRS_{i-1}] - 2[PRS_i]) \\ \frac{d[KAN1_i]}{dt} &= k_{b,KAN1} + v_{KAN1} \left(\frac{([KAN1_i])^2}{K_{KAN1 \rightarrow KAN1}} + \frac{([MP_i])^2}{K_{MP \rightarrow KAN1}} \right) \frac{1}{1 + \left(\frac{[KAN1_i]}{K_{KAN1 \rightarrow KAN1}} \right)^2 + \left(\frac{[MP_i]}{K_{MP \rightarrow KAN1}} \right)^2} \frac{1}{1 + \left(\frac{[REV_i]}{K_{REV \rightarrow KAN1}} \right)^2 + \left(\frac{[PRS_i]}{K_{PRS \rightarrow KAN1}} \right)^2} \\ &\quad - d_{KAN1} [KAN1_i] + D([KAN1_{i+1}] + [KAN1_{i-1}] - 2[KAN1_i]) \end{aligned} \right.$$

where $i = 1, 2, \dots, 6$ from time 0 to 24 hours; $i = 1, 2, \dots, 8$ from 24 to 48 hours; or $i = 1, 2, \dots, 10$ after 48 hours. The $[x_0]$ ($x = REV, MP, PRS$, or $KAN1$) is set to $[x_1]$, and $[x]$ in the last cell is equal to that in the neighboring cell. D is the diffusion coefficient. k_b, v, d are the basal production rate, the maximal production rate, and the degradation rate, respectively. The k_{MP} is the basal production rate of MP in the third and fourth cells, and $\chi_{\{3,4\}}(i)$ is the indicator function that is equal to 1 only when $i = 3$ or 4; $\{3,4\}, \{5,6\}$, and $\{7,8\}$ are chosen when the time is in $[0, 24]$ hours, $[24, 48]$ hours, and after

48 hours, respectively. The existence of k_{MP} indicates that there is a source producing the *MP* gene product consecutively in the third and fourth cells from the right-hand side, which ensures high levels of MP in these two cells. This system is based on the circuit in simulation 6, and the reaction term will disappear if the corresponding link is lacking. MP inhibiting KAN can be modeled by $\frac{1}{1 + \left(\frac{[MP_i]}{K_{MP \rightarrow KAN1}} \right)^2}$ which is multiplied directly to v_{KAN1} .

To identify the effect of MP on polarity formation, we simulated the dynamics of the above gene products but with different regulatory networks (simulations 1 to 6). In simulation 1, only REV and KAN1 are taken into consideration; in simulation 2, four additional regulatory relationships (mutual activation between *MP* and *PRS*, positive autoregulation of MP on its own gene expression, and the inhibitory influence of KAN1 on *PRS*) are considered; simulation 3 focuses on the network that couples the network in simulation 2 and the activating influence of MP on *REV*; the network in simulation 4 is constructed from the regulatory relationships included in simulation 3 and repression of *KAN1* by MP; simulation 5 is similar to simulation 4 except that MP is considered to positively regulate *KAN1*; the network in simulation 6 is based on the network from simulation 5, to which $REV \rightarrow MP, PRS \rightleftharpoons REV$, and $PRS \rightarrow KAN1$ are added. The initial states are set to form the adaxial-abaxial pattern: REV is set to 30 in the first three cells and 0 in the last three cells; KAN1 is set to 0 in the first three cells and 30 in the last three cells; PRS in six cells are set to be $[0, 0, 3, 3, 0, 0]$; MP is set to be $[20, 20, 40, 40, 20, 20]$ in all six cells. The kinetic parameters in the models are listed in table S2. We used ode15s in MATLAB to numerically simulate the dynamics on the time interval (0, 72 hours); at $t = 72$ hours, the steady state is obtained.

SUPPLEMENTARY MATERIALS

Supplementary material for this article is available at <https://science.org/doi/10.1126/sciadv.abn0368>

[View/request a protocol for this paper from Bio-protocol.](#)

REFERENCES AND NOTES

1. F. Du, C. Guan, Y. Jiao, Molecular mechanisms of leaf morphogenesis. *Mol. Plant* **11**, 1117–1134 (2018).
2. P. A. Conklin, J. Strable, S. Li, M. J. Scanlon, On the mechanisms of development in monocot and eudicot leaves. *New Phytol.* **221**, 706–724 (2019).
3. A. Maugarny-Calès, P. Laufs, Getting leaves into shape: A molecular, cellular, environmental and evolutionary view. *Development* **145**, dev161646 (2018).
4. A. Y. Husbands, D. H. Chitwood, Y. Plavskin, M. C. P. Timmermans, Signals and prepatterns: New insights into organ polarity in plants. *Genes Dev.* **23**, 1986–1997 (2009).
5. M. P. Caggiano, X. Yu, N. Bhatia, A. Larsson, H. Ram, C. K. Ohno, P. Sappl, E. M. Meyerowitz, H. Jönsson, M. G. Heisler, Cell type boundaries organize plant development. *eLife* **6**, e27421 (2017).
6. T. Yu, C. Guan, J. Wang, M. Sajjad, L. Ma, Y. Jiao, Dynamic patterns of gene expression during leaf initiation. *J. Genet. Genomics* **44**, 599–601 (2017).
7. R. K. Yadav, M. Perales, J. Gruel, C. Ohno, M. Heisler, T. Girke, H. Jönsson, G. V. Reddy, Plant stem cell maintenance involves direct transcriptional repression of differentiation program. *Mol. Syst. Biol.* **9**, 654 (2013).
8. D. S. Skopelitis, A. H. Benkovics, A. Y. Husbands, M. C. P. Timmermans, Boundary formation through a direct threshold-based readout of mobile small RNA gradients. *Dev. Cell* **43**, 265–273.e6 (2017).
9. C. Guan, B. Wu, T. Yu, Q. Wang, N. T. Krogan, X. Liu, Y. Jiao, Spatial auxin signaling controls leaf flattening in *Arabidopsis*. *Curr. Biol.* **27**, 2940–2950.e4 (2017).
10. M. Nakata, N. Matsumoto, R. Tsugeki, E. Rikirsch, T. Laux, K. Okada, Roles of the middle domain-specific *WUSCHEL-RELATED HOMEBOX* genes in early development of leaves in *Arabidopsis*. *Plant Cell* **24**, 519–535 (2012).
11. M. G. Heisler, C. Ohno, P. Das, P. Sieber, G. V. Reddy, J. A. Long, E. M. Meyerowitz, Patterns of auxin transport and gene expression during primordium development revealed by live imaging of the *Arabidopsis* inflorescence meristem. *Curr. Biol.* **15**, 1899–1911 (2005).

12. C. S. Galvan-Ampudia, G. Cerutti, J. Legrand, G. Brunoud, R. Martin-Arevalillo, R. Azais, V. Bayle, S. Moussu, C. Wenzl, Y. Jaillais, J. U. Lohmann, C. Godin, T. Vernoux, Temporal integration of auxin information for the regulation of patterning. *eLife* **9**, e55832 (2020).
13. D. Reinhardt, E. R. Pesce, P. Stieger, T. Mandel, K. Baltensperger, M. Bennett, J. Traas, J. Friml, C. Kuhlemeier, Regulation of phyllotaxis by polar auxin transport. *Nature* **426**, 255–260 (2003).
14. T. Vernoux, J. Kronenberger, O. Grandjean, P. Laufs, J. Traas, *PIN-FORMED 1* regulates cell fate at the periphery of the shoot apical meristem. *Development* **127**, 5157–5165 (2000).
15. H. Ram, S. Sahadevan, N. Gale, M. P. Caggiano, X. Yu, C. Ohno, M. G. Heisler, An integrated analysis of cell-type specific gene expression reveals genes regulated by *REVOLUTA* and *KANADI1* in the *Arabidopsis* shoot apical meristem. *PLOS Genet.* **16**, e1008661 (2020).
16. J. Shu, C. Wu, Y. Wu, Z. Li, S. Shao, W. Zhao, X. Tang, H. Yang, L. Shen, X. Zuo, W. Yang, Y. Shi, X. Chi, H. Zhang, G. Gao, Y. Shu, K. Yuan, W. He, C. Tang, Y. Zhao, H. Deng, Induction of pluripotency in mouse somatic cells with lineage specifiers. *Cell* **153**, 963–975 (2013).
17. F. Zhao, F. du, H. Oliveri, L. Zhou, O. Ali, W. Chen, S. Feng, Q. Wang, S. Lü, M. Long, R. Schneider, A. Sampathkumar, C. Godin, J. Traas, Y. Jiao, Microtubule-mediated wall anisotropy contributes to leaf blade flattening. *Curr. Biol.* **30**, 3972–3985.e6 (2020).
18. Z. Zhang, A. Runions, R. A. Mentink, D. Kierzkowski, M. Karady, B. Hashemi, P. Huijser, S. Strauss, X. Gan, K. Ljung, M. Tsiantis, A *WOX/auxin* biosynthesis module controls growth to shape leaf form. *Curr. Biol.* **30**, 4857–4868.e6 (2020).
19. N. Bhatia, B. Bozorg, A. Larsson, C. Ohno, H. Jönsson, M. G. Heisler, Auxin acts through *MONOPTEROS* to regulate plant cell polarity and pattern phyllotaxis. *Curr. Biol.* **26**, 3202–3208 (2016).
20. N. T. Krogan, D. Marcos, A. I. Weiner, T. Berleth, The auxin response factor *MONOPTEROS* controls meristem function and organogenesis in both the shoot and root through the direct regulation of *PIN* genes. *New Phytol.* **212**, 42–50 (2016).
21. D. R. Boer, A. Freire-Rios, W. A. M. van den Berg, T. Saaki, I. W. Manfield, S. Kepinski, I. López-Vidriero, J. M. Franco-Zorrilla, S. C. de Vries, R. Solano, D. Weijers, M. Coll, Structural basis for DNA binding specificity by the auxin-dependent ARF transcription factors. *Cell* **156**, 577–589 (2014).
22. R. Heidstra, D. Welch, B. Scheres, Mosaic analyses using marked activation and deletion clones dissect *Arabidopsis* SCARECROW action in asymmetric cell division. *Genes Dev.* **18**, 1964–1969 (2004).
23. M. Cole, J. Chandler, D. Weijers, B. Jacobs, P. Comelli, W. Werr, *DORNROSCHEN* is a direct target of the auxin response factor *MONOPTEROS* in the *Arabidopsis* embryo. *Development* **136**, 1643–1651 (2009).
24. M. Vandenbussche, A. Horstman, J. Zethof, R. Koes, A. S. Rijpkema, T. Gerats, Differential recruitment of *WOX* transcription factors for lateral development and organ fusion in *Petunia* and *Arabidopsis*. *Plant Cell* **21**, 2269–2283 (2009).
25. D. Otsuga, B. DeGuzman, M. J. Prigge, G. N. Drews, S. E. Clark, *REVOLUTA* regulates meristem initiation at lateral positions. *Plant J.* **25**, 223–236 (2001).
26. J. F. Emery, S. K. Floyd, J. Alvarez, Y. Eshed, N. P. Hawker, A. Izhaki, S. F. Baum, J. L. Bowman, Radial patterning of *Arabidopsis* shoots by class III HD-ZIP and *KANADI* genes. *Curr. Biol.* **13**, 1768–1774 (2003).
27. T.-T. Xu, S.-C. Ren, X.-F. Song, C.-M. Liu, *CLE19* expressed in the embryo regulates both cotyledon establishment and endosperm development in *Arabidopsis*. *J. Exp. Bot.* **66**, 5217–5227 (2015).
28. A. Schlereth, B. Möller, W. Liu, M. Kientz, J. Flipse, E. H. Rademacher, M. Schmid, G. Jürgens, D. Weijers, *MONOPTEROS* controls embryonic root initiation by regulating a mobile transcription factor. *Nature* **464**, 913–916 (2010).
29. R. Brandt, M. Salla-Martret, J. Bou-Torrent, T. Musielak, M. Stahl, C. Lanz, F. Ott, M. Schmid, T. Greb, M. Schwarz, S. B. Choi, M. K. Barton, B. J. Reinhart, T. Liu, M. Quint, J. C. Palauqui, J. F. Martínez-García, S. Wenkel, Genome-wide binding-site analysis of *REVOLUTA* reveals a link between leaf patterning and light-mediated growth responses. *Plant J.* **72**, 31–42 (2012).
30. Y. Han, C. Zhang, H. Yang, Y. Jiao, Cytokinin pathway mediates *APETALA1* function in the establishment of determinate floral meristems in *Arabidopsis*. *Proc. Natl. Acad. Sci. U.S.A.* **111**, 6840–6845 (2014).
31. X. Cao, J. Wang, Y. Xiong, H. Yang, M. Yang, P. Ye, S. Bencivenga, R. Sablowski, Y. Jiao, A self-activation loop maintains meristematic cell fate for branching. *Curr. Biol.* **30**, 1893–1904.e4 (2020).
32. B. Shi, C. Zhang, C. Tian, J. Wang, Q. Wang, T. Xu, Y. Xu, C. Ohno, R. Sablowski, M. G. Heisler, K. Theres, Y. Wang, Y. Jiao, Two-step regulation of a meristematic cell population acting in shoot branching in *Arabidopsis*. *PLOS Genet.* **12**, e1006168 (2016).

Acknowledgments: We thank M. Heisler, C.-M. Liu, E. Meyerowitz, and G. Venu Reddy for materials. **Funding:** This work was supported by NSFC grant 31825002, the K.C. Wong Education Foundation, NSFC grant 31872835, NSFC grant 12050002, National Key R&D Program of China 2021YFF1200500, and Bureau of National Tobacco grant 110202001021 (JY-04). **Author contributions:** Conceptualization: Y.J. Methodology: C.G., L.Q., and Y.X. Investigation: C.G., L.Q., and Y.X. Funding acquisition: L.Z. and Y.J. Project administration: L.Z. and Y.J. Supervision: L.Z. and Y.J. Writing—original draft: C.G., L.Q., L.Z., and Y.J. Writing—review and editing: C.G., L.Q., L.Z., and Y.J. **Competing interests:** The authors declare that they have no competing interests. **Data and materials availability:** All data needed to evaluate the conclusions in the paper are present in the paper and/or the Supplementary Materials.

Submitted 29 October 2021

Accepted 22 April 2022

Published 8 June 2022

10.1126/sciadv.abn0368